RSC Publishing Faraday Discussions

# DFT calculation of oxygen adsorption on platinum nanoparticles: Coverage and size effects



| | |
|---|---|
| Journal: | *Faraday Discussions* |
| Manuscript ID | Draft |
| Article Type: | Paper |
| Date Submitted by the Author: | n/a |





| | |
|---|---|
| Complete List of Authors: | GARCIA VERGA, LUCAS; University of Southampton, Chemistry<br>Aarons, Jolyon; University of Southampton, Chemistry<br>Sarwar, Misbah; Johnson Matthey Technology Centre,<br>Thompsett, David; Johnson Matthey plc, Johnson Matthey Technology Centre<br>Russell, Andrea; University of Southampton, Department of Chemistry<br>Skylaris, Chris-Kriton; University of Southampton, Chemistry |

Journal Name

ARTICLE TYPE

Cite this: DOI: 10.1039/xxxxxxxxxx

# DFT calculation of oxygen adsorption on platinum nanoparticles: Coverage and size effects †

L.G. Verga,[a] J. Aarons,[a] M. Sarwar,[b] D. Thompsett,[b] A.E. Russell,[a] and C-K. Skylaris[a*]

Received Date
Accepted Date

DOI: 10.1039/xxxxxxxxxx

www.rsc.org/journalname

Catalysts made of Pt nanoparticles and Pt alloys are considered state-of-the-art catalysts for the anodic and cathodic reactions involved in hydrogen fuel cells. The optimal size of such nanoparticles for each chemical reaction is an unsolved problem, which depends on environmental variables, such as reactant concentration, solvent, temperature, etc[1,2]. From a theoretical point of view, this problem has been tackled mainly by observing how single key adsorbates react with different nanoparticles in controlled conditions. In this work, we use large-scale DFT calculations to examine the interplay between the Pt nanoparticle size and O coverage effects. We examine single O adsorptions for three adsorption sites on cuboctahedral platinum nanoparticles with different sizes. As we grow the nanoparticle size, the binding strength decreases and we observed a quick convergence of the adsorption energies with increasing nanoparticle size, which correlates with the calculated d-band centre for (111) Pt facets on such nanoparticles. We also carried out a detailed study of the effect of oxygen coverage with varying fractions of O monolayer coverage, computing adsorption energies per O atom for $Pt_{55}$, $Pt_{147}$, and $Pt_{309}$ nanoparticles with several O coverages. In general, the increase of O coverage led to weaker adsorption energies per O atom, and when analysing the results in terms of oxygen monolayers, this effect is more pronounced for larger nanoparticles. The O coverage dependency of the adsorption energy per O atom is analysed in terms of the O distribution for each nanoparticle size and electronic changes that the adsorbed oxygen causes to the Pt nanoparticle. In studying nanoparticle size and oxygen coverage effects simultaneously, we offer insights with DFT accuracy to help on heterogeneous catalyst design.

## 1 Introduction

Rational heterogeneous catalyst design is one of the main research challenges in physical chemistry due to the high number of industrial and environmental applications which rely on the efficiency, activity and selectivity of such catalysts. The catalyst efficiency is a key variable for $CO_2$ reduction, conversion of biomass to hydrogen and other fuels, sulphur removal from combustible fuels, and other chemical processes crucial in our drive for a sustainable society. For instance, the fuel cell technology can be a valuable tool for lowering pollutant emissions, because fuel cells are capable of producing electricity safely and with high autonomy. However, fuel cell performance depends on catalysts able to perform anodic and cathodic reactions efficiently.

A deeper understanding of how the catalyst surfaces interact with reactants, products and intermediates is fundamental to design new catalysts for each reaction. Consequently, computational studies developed with density functional theory (DFT) and molecular dynamics (MD) on atomic and molecular adsorptions on catalytic surfaces are simple and powerful tools to provide insights at the atomic level the ability of certain metallic surfaces to act as catalysts for specific chemical reactions.

First of all, atomic and molecular adsorptions are usually the first step towards chemical reactions on the catalyst surface. Secondly, by exploiting the Sabatier principle[3], DFT calculations of adsorption energies have enabled researchers to create scaling relations between bond energies and reaction barriers, generating the so-called volcano plots which can be tested both theoretically and experimentally and be used to predict new catalysts. As an example, Jacobsen *et al.*[4] correlated via DFT calculations the adsorption energy of atomic N with the production rate of ammonia using different materials, showing a remarkable correlation between experimental and theoretical data and concluding that CoMo alloys should be efficient catalysts for this reaction. Similarly, the atomic oxygen adsorption energy correlates with the re-

[a] *Department of Chemistry, University of Southampton, Highfield, Southampton SO17 1BJ, United Kingdom*
[b] *Johnson Matthey Technology Centre, Blounts Court, Reading, Berkshire, UK RG4 9NH*
* *E-mail: c.skylaris@soton.ac.uk*

† Electronic Supplementary Information (ESI) available: [details of any supplementary information available should be included here]. See DOI: 10.1039/b000000x/

action energy of oxygen reduction reactions (ORR) in the form of a volcano plot[5–7]. Atomic oxygen adsorption energies were also used to describe to some extent chemical reactions such as the C-C, C-H, and C-O bond breaking in the ethanol steam reforming[8], and CO hydrogenation[9].

Recently, Abild-Pedersen *et al.*[10] showed with DFT calculations, that it is possible to predict the adsorption of polyatomic molecules using atomic adsorptions as descriptors. They demonstrated that the adsorption energy of $CH_x$, $OH_x$, $NH_x$, and $SH_x$ can be predicted by using the adsorption energies of C, N, O, and S atoms. This discovery led to further scaling relations, such as the ones observed by Liu and Greeley[11], correlating the adsorption energies of several intermediates in the glycerol oxidation with the adsorption energies of O, C, and glycerol itself. The adsorption energies of glycerol and intermediates can describe the reaction barriers in the glycerol oxidation reaction[11] via the Brønsted-Evans-Polanyi principle. Thus, the correlation between energy barriers and adsorption energies, and the scaling relations between the adsorption energy of polyatomic molecules and atoms can drastically reduce the computational effort necessary to study such complicated reactions.

Computing the adsorption energies for a wide range of metal surfaces and alloys, crystal facets, nanoparticle shapes and sizes, and adsorption sites is a highly computationally demanding task. Thus, considerable effort has been applied to finding electronic and geometrical properties in the catalyst material to describe and predict the adsorption energies of atoms and molecules. Nørskov *et al.* showed that the ability of a catalyst surface to adsorb atomic oxygen correlates to the energetic centre of the d-band in comparison with the Fermi level[5,12,13], showing that as the d-band centre shifts to values closer to the Fermi level, the oxygen adsorption energy strengthens.

The d-band centre descriptor has been widely tested and validated throughout the last years for different adsorbates and catalytic surfaces. Moreover, geometric and electronic changes in the catalytic surface, such as the ones caused by alloying metals or using different supports for metallic monolayers and nanoparticles[14–20], have been correlated with d-band centre shifts and catalyst reactivity, providing insights about general guidelines to control the catalytic activity of metallic surfaces. Recently, new descriptors have been developed and tested for atomic and molecular adsorption. For example, Calle-Vallejo *et al.*[21] showed that the generalized coordination number, a purely geometric descriptor, predicts the adsorption energies for different adsorption sites and nanoparticle sizes successfully without the need of a single electronic structure calculation. Aarons *et al.*[22] also describe the atomic oxygen adsorption energies on different adsorption sites of Pt nanoparticles by using a descriptor which relies on the local value of the electronic density.

Most of the computational studies on oxygen adsorption on metallic surfaces treat the problem in the low O coverage limit, as the system complexity and computational cost of such simulations grow with the number of atoms. However, the adsorption energies are dependent on the adsorbate coverage due to the adsorbate-adsorbate interactions and the electronic and geometric changes that the adsorbates induce in the catalytic surface. Miller and Kitchin[23] studied the effect of atomic oxygen coverage for Pt and Au fcc (111) surfaces, observing a weakening in the adsorption energies with the increase in the oxygen coverage. They showed that the increase in the oxygen coverage induces electronic changes in the metallic surfaces with a broadening of the d-band of surface atoms and a downshift in the d-band centre energies[23]. A coverage dependence of the adsorption energies associated with changes in the d-band centre due to the adsorbates presence was also found for Pd (111) facets and atomic C, N and O[24] and corroborated on different metallic slabs[25–27].

Meanwhile, Bray, Skavdahl, McEwen, and Schneider[28] showed that the O adsorption with increasing adsorbate coverage is highly dependent on the O cluster configuration, which can be tuned with cluster expansions methods[28–32], and was a key variable to reproduce temperature programmed desorption experiments with first principle calculations[28]. Getman and Schneider[30] and Frey, Schmidt, Wolverton, and Schneider[31] also showed the importance and non-uniformity of surface coverage effects on the activation energies of different reaction steps in the NO oxidation reaction. Bray, Smith and Schneider[32] also studied a stepped, kinked Pt (321) surface as a better model for metallic nanoparticles. They showed that on Pt (321) surfaces, atomic oxygen binds preferentially at bridge sites at the step edges for low O coverages, and as the coverage increases O also adsorbs on threefold hollow sites forming $PtO_4$-like structures.

Most of the catalysts used for fuel cell applications are made from expensive materials such as Pt, Pd, Rh, and Au. Aiming to increase the active surface area per mass, pure and alloyed metallic nanoparticles have been used in state-of-the-art catalysts. For metallic nanoparticles, it is possible to control the catalytic activity by changing parameters such as size, composition and shape, which creates additional paths to search for optimal catalysts. For instance, Pt nanoparticles catalysts have peaks of mass activity usually around 2.5 nm diameter[33–36]. Also, for metallic nanoparticles, adsorption sites on the edges and vertices of the nanoparticles are present, and the interaction of adsorbates with such sites is dramatically different from the ones observed on (111) or (100) facets.

Computational studies performed with DFT on size effects for Pt nanoparticles are usually carried out in the low coverage approximation. For instance, Han, Miranda, and Ceder[37] studied via DFT OH and O adsorptions on Pt nanoparticles with up to (number) atoms showing the following adsorption site hierarchy: bridge vertex < hollow-HCP < top vertex < hollow-FCC < bridge centre < top edge. They also showed a weakening in the adsorption energy with the Pt nanoparticle increase[37], which was also demonstrated by Li *et al.*[38] for the interaction of O with Pt nanoparticles.

Studying adsorbate coverage effects on metallic nanoparticles with computational simulations is a demanding task. However, it is still possible to find a few studies carried out with DFT and MD calculations on this subject. As an example, Wei and Liu[33] observed with DFT calculations that the O coverage for Pt nanoparticles is much higher at edge adsorption sites than at the terrace sites at (111) facets and that the oxidation on Pt nanoparticles should start in the nanoparticle edges. Also, the coverage on

(100) facets is higher than the one observed on (111) facets[33].

Jinnouchi, Suzuki, and Morimoto[39] also studied the coverage dependency with DFT calculations, showing that Pt electrooxidation starts with the adsorption of OH adsorbates at adsorption sites near the edges of the nanoparticles. With increasing electrode potential, atomic O replaces OH species, and as the edges and corners of the nanoparticles are easily covered with O, these sites become inactive for ORR and are the starting points for catalyst corrosion, which can be avoided by doping edges of Pt nanoparticles with Au atoms[39]. Jinnouchi, Suzuki, and Morimoto[39] also observed that at high O coverage, some oxygen atoms move to subsurface sites. Subsurface oxygen with increasing O coverage was also observed experimentally[40,41], and with MD calculations[42], and with DFT calculations for Pt slabs[43]. The presence of subsurface oxygen is an important phenomenom on catalysis research, as it is associated with the Pt catalyst corrosion and changes in the catalyst surface reactivity[40,41,44].

Recently, Gai *et al.*[42] studied the effects of oxygen coverage for Pt catalysts via MD calculations on Pt surfaces and nanoparticles of different sizes and shapes. For spherical Pt nanoparticles of various sizes, they observed that hollow sites are the first to adsorb O, followed by subsurface sites. Smaller nanoparticles formed bulk oxides at lower pressures as compared with the larger clusters, which was explained due to the decrease on O adsorption surface sites on smaller nanoparticles and to the higher percentage of edge and corners sites which adsorb O more easily. The effect of the rate of edges and corners was also demonstrated by comparing different Pt nanoparticles shapes, where octahedron models with a higher percentage of edges and corners showed higher oxygen coverages when compared with cubic and cuboctahedral models[42].

Here, we will provide details about the implementation of an angular momentum projected density of states with the ONETEP linear-scaling DFT formalism[45], which is useful to catalyst research to calculate the d-band centres that act as an electronic descriptor. We compute with large-scale DFT calculations atomic O adsorption energies for $Pt_n$ nanoparticles with $n$ up to 309 atoms in different adsorption sites. We also show a detailed analysis of different methodologies used to tackle the oxygen coverage problem with DFT calculations, showing the limits of each approximation made to reduce the computational cost. The chosen methodology is then used to study the complicated interplay between O coverage and Pt nanoparticle size, by computing different O coverages for three nanoparticle sizes. We discuss and interpret these results in terms of oxygen adsorption energies, O distribution for each coverage and electronic structure changes induced in the Pt surfaces due to the interaction with the adsorbates.

In the next section we describe the computational methods used for our calculations. Next, we describe our implementation of a angular momentum projected density of states (p-DOS) in the ONETEP code[45]. We then show our results for single atomic oxygen adsorptions and for a series of oxygen coverages in cuboctahedral platinum nanoparticles of increasing size. Finally, we present our conclusions about the obtained results aiming to provide insights about these effects for practical catalyst design.

## 2 Methods

We performed our DFT calculations with the ONETEP linear-scaling DFT program[45] within the ensemble-DFT (EDFT) method[46], which allows large-scale DFT calculations on metallic systems. In ONETEP, the density matrix is constructed with localised non-orthogonal generalised Wannier functions (NGWFs)[47] and a density kernel matrix, as follows:

$$\rho(\vec{r},\vec{r'}) = \sum_{\alpha\beta} \phi_\alpha(\vec{r}) K^{\alpha\beta} \phi^*{}_\beta(\vec{r'}) \quad (1)$$

where $\rho$ is the one particle electronic density matrix, $\phi$ is a NGWF, and $K^{\alpha,\beta}$ is the density kernel matrix, which is a generalisation of state occupancy to the NGWFs. The NGWFs are expanded in terms of psinc basis functions[48], which are equivalent to a plane wave basis set, and are optimised in situ, allowing variational freedom and results with near-complete basis set accuracy.

We adopted the rPBE functional[49] as our exchange-correlation functional, which is known to be particularly good for calculations of binding energies on surfaces[50], and the projector augmented wave (PAW) method[51,52] to represent the core electrons.

We set the psinc basis set kinetic energy cutoff to 550 eV for geometry optimisations and 850 eV for total energy and properties calculations. We assigned 12 NGWFs for each Pt atom and 4NGWFs for each O atom. For all NGWFs, we used 9.0 $a_0$ radii. The NGWF conjugate gradient optimisation preconditioning parameter $k_0$[53] used in our simulations was equal to 2.5 $a_0{}^{-1}$. The Fermi-Dirac occupancy smearing scheme was used, with a 0.1 eV electronic temperature.

We used simulation cells obeying periodic boundary conditions with large vacuum gaps and with the spherical Coulomb-cutoff approach to eliminate interactions between periodic images[54]. In the supplementary information, we show a convergence test for Coulomb-cutoff radius[†]. We calculate the minimum Coulomb-cutoff radius $r_{CC}$ with the following equation:

$$r_{CC} = rmax_{ij} + 2r_{NGWF} + a \quad (2)$$

where $rmax_{ij}$ is the maximum inter-atomic separation in our systems, $r_{NGWF}$ is the NGWF radius, and $a$ is a constant value of at least 5 Å to account for Gibbs oscillations associated with the cut-off in the Coulomb operator.

We employed the BFGS method to optimise the geometries[55], using a convergence threshold of 0.002 Eh/$a_0$ on the atomic forces for the optimisation of O on Pt nanoparticles and 0.005 Eh/$a_0$ for the optimisation of isolated Pt nanoparticles. On the next sections, we discuss in details different geometry optimisations strategies to study the O adsorption for different nanoparticle sizes and O coverages.

## 3 Angular momentum projected density of states

The d-band model, proposed by Nørskov *et al*[5,12,13], is an important tool for catalyst design using computational simulations, as it provides a mechanism to qualitatively predict and interpret ad-

sorption energies of several ligands on transition metal surfaces, which can be used to predict catalytic activity. This model is built under the observation that chemisorption of ligands can be described through the interaction between the s and d states in the metallic surface and the valence states from the ligand.

The contribution from the interaction of the metallic s band and the ligand s and p orbitals is very similar over transition metals, as the s energy levels of metallic surfaces form delocalised and continuum bands which do not vary much between different surfaces. On the other hand, the d levels of metallic surfaces are comparatively localised and are considered, under the d-band model, to be responsible for the main variations in the adsorption energies of ligands on different surfaces.

The interaction between ligands and the metal d-band arise from the formation of bonding and anti-bonding states between adsorbate and metal surface. The filling of the anti-bonding state controls the bonding strength and it can be evaluated through the energy of the anti-bonding state in comparison with the Fermi level. As the energy of the anti-bonding state is always higher than the energy of the d states, Nørskov proposed that the energetic centre of the occupied d-band relative to the Fermi level can be a good descriptor of anti-bonding state energy, and consequently the anti-bonding state filling and the bonding strength. Thus, higher d-band centres with respect to the Fermi level in metallic surfaces are associated with stronger ligand adsorption energies.

To calculate the d-band centre, one has to be able to calculate the density of states of the metallic system for each angular momentum, as the d-band centre with respect to the Fermi level $\varepsilon_d - \varepsilon_f$, is defined as the average energy of the d-electrons.

$$\varepsilon_d - \varepsilon_f = \frac{\int \varepsilon \rho_d(\varepsilon) f(\varepsilon)\, d\varepsilon}{\int \rho_d(\varepsilon) f(\varepsilon)\, d\varepsilon}, \tag{3}$$

where $\rho_d(\varepsilon)$, is the DOS of the d electrons, either for all atoms or for a subset of the atoms as in the cases when we are interested in studying a metallic surface, and $f(\varepsilon)$ is the occupancy of the bands at energy $\varepsilon$. The density of states (DOS) is a function of the energy $\varepsilon$ defined as:

$$\rho(\varepsilon) = \sum_i \langle \psi_i | \psi_i \rangle \delta(\varepsilon - \varepsilon_i), \tag{4}$$

where $\varepsilon_i$ are the eigenvalues of the Hamiltonian, or band energies, and $\psi_i$ are the eigenfunctions or bands.

In ONETEP, the electron bands $\psi_i(\vec{r})$ are written in terms of NGWFs $\phi_\alpha(\vec{r})$ using the eigenvalues of the one-particle Hamiltonian:

$$\psi_i(\vec{r}) = \phi_\alpha(\vec{r}) M^\alpha{}_i, \tag{5}$$

where we use the summation convention over repeated Greek letter indices, that correspond to non-orthogonal quantities. In terms of the NGWFs the normalisation condition of the bands becomes:

$$M^\dagger{}_i{}^\alpha \langle \phi_\alpha | \phi_\beta \rangle M^\beta{}_i = 1. \tag{6}$$

In order to compute a projected density of states such as $\rho_d(\varepsilon)$ in ONETEP, the NGWFs need to be projected onto basis functions with angular momentum resolution and for this purpose we use sets of spherical waves with the same centres and localisation as the NGWFs. In addition to the projection to angular momentum we would like to partition each eigenvalue into contributions associated with a subset of atoms, creating a local and angular momentum projected DOS. To give angular momentum and atomic resolution, we can insert a basis of truncated spherical waves,

$$\chi_{A,k_{n,l},l,m}(\vec{r}) = j_l(kr) Y_{l,m}(\Omega) H(a-r), \tag{7}$$

where $A$ represents an atom, $n$,$l$ and $m$ are the quantum numbers, $j_l$ are spherical Bessel functions of the first kind, $Y_{l,m}$ are the spherical harmonics and $\Omega$ is the solid angle corresponding to $\vec{r}$. H is the Heaviside step function used to truncate the spherical waves inside spheres with radii $a$.

We can choose at this point either to use the full set of spherical waves on each atomic centre within a given psinc kinetic energy cut-off or to contract to a smaller set of functions. We call these spherical wave contracted functions (SWCFs):

$$\chi_{A,l,m_l}(\vec{r}) = \sum_k \omega_k \chi_{A,k_{n,l},l,m_l}(\vec{r}), \tag{8}$$

where $\omega_k$ are weights which in practice are unity. An identity operator in terms of the SWCFs can be constructed as follows:

$$\hat{1} = |\chi_{A,l,m}\rangle O^{A,l,m|B,l',m'} \langle \chi_{B,l',m'}| \tag{9}$$

where an implicit summation is assumed over repeated indices and $O^{A,l,m|B,l',m'}$ is the inverse overlap matrix of the SWCFs. By inserting (6) and (9) in equation 4 we obtain an decomposition of the DOS in terms of atoms and angular momentum channels:

$$\rho(\varepsilon) = \sum_i M_i^{\dagger\alpha} \langle \phi_\alpha | \phi_\beta \rangle M^\beta{}_i \, \delta(\varepsilon - \varepsilon_i) \tag{10}$$

$$\rho(\varepsilon) = \sum_i M_i^{\dagger\alpha} \langle \phi_\alpha | \chi_{A,l,m} \rangle O^{A,l,m|B,l',m'} \langle \chi_{B,l',m'} | \phi_\beta \rangle M^\beta{}_i \, \delta(\varepsilon - \varepsilon_i) \tag{11}$$

$$\rho(\varepsilon) = \sum_i R_i^{B,l',m'} T_{B,l',m',i} \, \delta(\varepsilon - \varepsilon_i) \tag{12}$$

where the quantities $R_i^{B,l',m'}$ and $T_{B,l',m',i}$ are defined from the above equation. We can then define a set of weights as the Hadamard product of R and the transpose of T, so that finally the full DOS becomes

$$\rho(\varepsilon) \quad = \quad \sum_{B,l',m',i} W_{(B,l',m'),i} \, \delta(\varepsilon - \varepsilon_i) \tag{13}$$

The above expression allows us full flexibility to process the DOS according to our requirements by using the matrix of weights $W_{(B,l',m'),i}$ allows us to construct various types of DOS. For example, in order to construct the DOS for the d electrons we can add up all the weights for $l' = 2$ while if we want to restrict this DOS to a subset of atoms of our system (such as only the atoms on a surface $\mathscr{S}$) we can further restrict the summation to only these

atoms:

$$\rho_{d,\mathscr{S}}(\varepsilon) = \sum_{B\in\mathscr{S},m',i} W_{(B,2,m'),i}\,\delta(\varepsilon-\varepsilon_i)\ . \qquad (14)$$

This expression was derived for the case of norm-conserving pseudopotentials where $\psi_i$ are the pseudo wavefunctions. In the case of PAW calculations[51,52], equation 4 becomes

$$\rho(\varepsilon) = \sum_i \langle\tilde{\psi}_i|\hat{\tau}^\dagger\,\hat{\tau}|\tilde{\psi}_i\rangle\delta(\varepsilon-\varepsilon_i), \qquad (15)$$

where $\tilde{\psi}_i$ are the smooth valence wavefunctions and $\hat{\tau}$ is the PAW operator that transforms these to the valence wavefunctions with all-electron shapes in the core. This results in replacing the integrals $\langle\chi_{B,l',m'}|\phi_\beta\rangle$ with $\langle\chi_{B,l',m'}|\hat{S}|\phi_\beta\rangle$ where $\hat{S}$ is the overlap operator (unity operator) in the PAW formalism[51,52]. These integrals are evaluated using the existing PAW machinery of ONETEP.

Finally, the number of electrons that occupy a particular DOS can be obtained as the area under the DOS multiplied by the occupancy, so for the example of equation 14 we would obtain the number of electrons as follows:

$$N_e(d,\mathscr{S}) = \int f(\varepsilon)\rho_{d,\mathscr{S}}(\varepsilon)\,d\varepsilon \qquad (16)$$

provided of course that the weights have been normalised appropriately, so that

$$N_e = \sum_{A,l,m,i} W_{(A,l,m),i} f(\varepsilon_i) \qquad (17)$$

is the total number of electrons.

We plot on Figure 1 the total and the projected density of states for an O atom on a singlet state and a CO molecule. We performed the calculations using the same parameters described in the previous section. For CO, we optimised the molecule geometry before running the properties calculation.

For the O atom, it is simple to observe that the density of states was successfully projected to s and p orbitals. For the CO molecule, the total DOS shows the existence of four peaks, representing the occupied molecular orbitals formed by the valence electrons. The last and the first two peaks represent $\sigma$ orbitals formed by hybridised sp orbitals and are described in our angular momentum projected density of states as a sum of s and p contributions. The third peak is two times more intense, as it represents two degenerate $\pi$ molecular orbitals which are, as expected, fully projected as a p band, illustrating the results we can obtain with the implementation of the angular momentum projected density of states.

## 4 Results

### 4.1 Size effects for single O adsorption

In this section, we present how the adsorption energies for a single oxygen atom change as we increase the Pt nanoparticle size. We start our calculations by geometry optimising the Pt nanoparticles, which will remain fixed in the optimised structure during the geometry optimisation of the adsorbate on top of the nanoparticle. We calculate the adsorption energies, $E_{ADS}$, as follows:

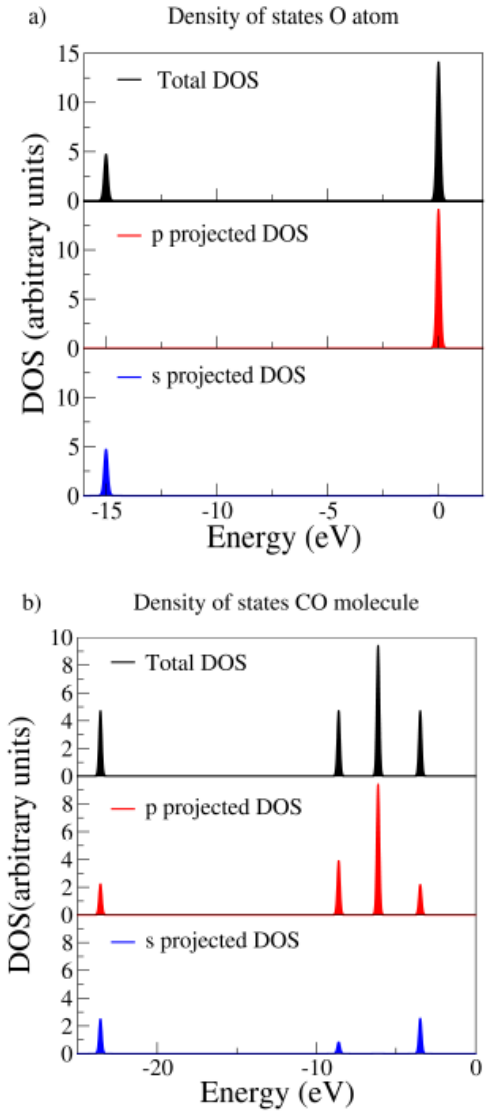


**Fig. 1** Total and projected density of states for a) an O atom in a singlet state and b) a CO molecule. Blue and red plots represent s and p bands, while black curves are obtained with the total DOS.

$$E_{ADS} = E_{O/Pt_n} - E_{Pt_n} - \frac{1}{2}E_{O_2} \qquad (18)$$

where, $E_{O/Pt_n}$ is the energy for the system with O interacting with a Pt nanoparticle, $E_{Pt_n}$ is the energy of the Pt nanoparticle, and $E_{O_2}$ is the energy of an oxygen molecule in the triplet state. Figure 2 shows the adsorption sites we used for single atomic oxygen adsorption.

We calculated O adsorption at the hollow HCP and hollow FCC sites, respectively near the vertex and centre of the (111) nanoparticle facet. For the (100) facet, we calculated the adsorption energies for bridge sites near the edge of the nanoparticle.

Figure 3 shows adsorption energies as a function of the nanoparticle size. For the (111) facet, HCP hollow binds O stronger than the FCC (111), this result agrees with observations previously obtained for Pt nanoparticles[37,56,57] and it is the opposite of the observed for Pt slabs[43], due to the proximity of HCP

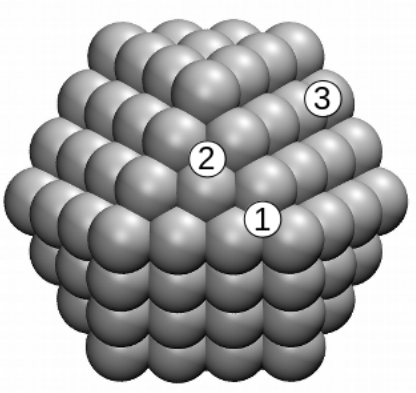


**Fig. 2** Adsorption sites for oxygen on a $Pt_{147}$ cuboctahedral nanoparticle, where 1,2 and 3 are, respectively, HCP, FCC, and Bridge (100) adsorption sites.

sites and the edges of the nanoparticles.

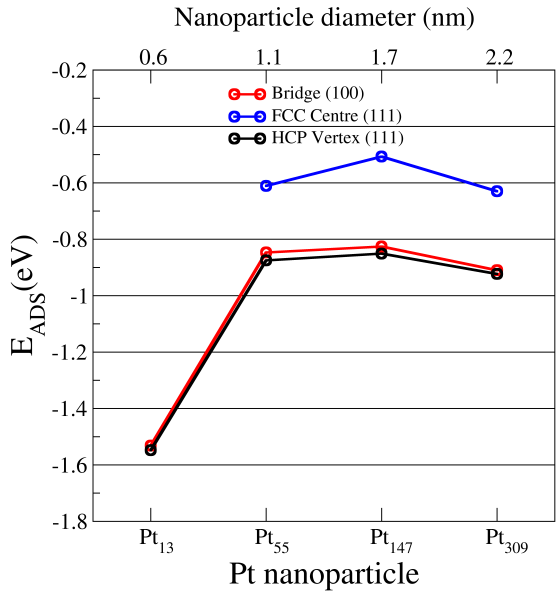


**Fig. 3** Adsorption energies for O interacting with $Pt_n$ nanoparticles with up to 309 atoms, with oxygen atoms placed at HCP (black) and FCC (red) adsorption sites for the (111) facet, and Bridge (blue) for the (100) facet. For $Pt_{13}$, there is no data available for FCC (111), as this adsorption site is not present.

We also observe that the adsorption energy obtained for hollow (HCP) on (111) facets is similar to the observed for bridge (100) near the edge of the nanoparticle. This result also agrees with previous papers[37], and it will be used to guide us in our studies regarding O coverage effects.

For all adsorption sites, the O adsorption weakens as we increase the nanoparticle size, which agrees with previous observations in the literature. For nanoparticles larger than $Pt_{55}$, the variations in the adsorption energies are smaller than 0.10 eV. The fast convergence of O adsorption energies within the Pt nanoparticle size and the subtle peak for Pt nanoparticles near 1.7 *nm* is also similar to that observed in previous works from Li. *et.al*[38] for cuboctahedral nanoparticles and from Shao, Peles, and Shoemaker[36] for truncated octahedral nanoparticles.

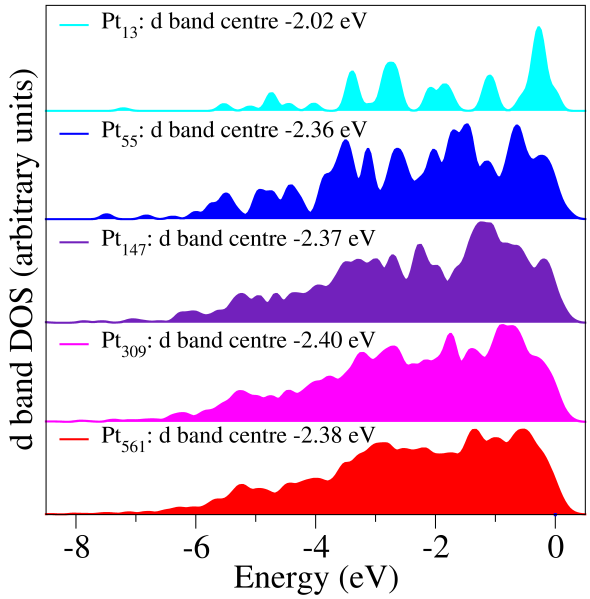


**Fig. 4** Angular momentum projected density of states on (111) facets of cuboctahedral $Pt_n$ nanoparticles with $13 \leq n \leq 561$.

Figure 4 shows the d-band projected density of states for (111) facets of Pt nanoparticles ranging from 13 to 561 atoms. The d-band projected density of states of Pt (111) facets vary with nanoparticle size in a similar way that the O adsorption energies do. As we increase the nanoparticle size, the d-band states become more continuous and converge towards the results of the largest nanoparticle size. As expected, with increasing nanoparticle sizes, the d-band centre shifts away from the Fermi level, which is associated to weaker O binding, quickly converging to the value obtained for our largest nanoparticle, with the difference in the d-band centre for all nanoparticles sizes between $Pt_{55}$ and $Pt_{561}$ being smaller than 0.05 eV. As the d-band centre for $Pt_{561}$ is similar to the obtained for all nanoparticles larger than $Pt_{55}$, we do not expect any significant change in the O adsorption energies for this nanoparticle size.

### 4.2 Coverage effect: Methodology calibration

Studying the oxygen coverage effect on Pt nanoparticles of different sizes with DFT calculations is a highly computationally demanding task. This section aims to thoroughly describe approximations made to reduce the computational effort, and assess the validity of each model and the limits of our results. Finding the ground state arrangements of O atoms for each coverage can be a complicated task. In the literature, some authors have analysed the importance of oxygen arrangements for each coverage for Pt surfaces[28–32]. When treating Pt nanoparticles, this task is even more complicated due to the increase of adsorption sites, because the proximity of an adsorption site to the edge of the nanoparticle changes its capacity of adsorbing oxygen.

Here, we started our simulations with O atoms placed at hollow HCP and bridge sites near the edge of the nanoparticle for (111) and (100) facets respectively. These adsorption sites are

the stronger ones for each nanoparticle facet if we ignore the adsorption sites in the edges or vertex of the nanoparticle. As the adsorption energies for HCP (111) and bridge (100) are similar in the single oxygen limit, we assumed an even increase in oxygen coverage on both facets.

We studied cuboctahedral platinum nanoparticles with up to 309 Pt atoms, covering the nanoparticles with up to 1ML of oxygen atoms, where we define 1 ML coverage if the number of O atoms is the same as the number of Pt surface atoms. To reduce the computational cost associated with the increasing number of O atoms, we performed our O coverage calculations under three assumptions:

I) Constraining Pt nanoparticle movement.

The first assumption is widely used when studying the adsorption of atoms and molecules on metallic nanoparticles with DFT calculations. We assume that the change in the adsorption energy due to the nanoparticle deformation after the interaction with the adsorbate should be small and would create a near constant shift on adsorption energies, not changing overall trends and main conclusions when comparing different systems.

To test this assumption, we compute the adsorption energies per O atom with two geometry optimisation strategies, here called "Relaxing Pt", when we geometry optimise all the Pt and oxygen atoms, and "Freezing Pt" when we optimise only O atoms with the Pt atoms constrained.

We computed single O adsorption and multiple O adsorptions varying the oxygen coverage for $Pt_{55}$ and $Pt_{147}$ nanoparticles. For $Pt_{55}$ nanoparticles we tested the assumption for systems with the whole nanoparticle covered and with only one hemisphere covered, while for $Pt_{147}$ we only considered hemispherical coverages. We calculate the adsorption energy per O atom as follows:

$$E_{ADS} = E_{O_m/Pt_n} - E_{Pt_n} - \frac{m}{2}E_{O_2} \quad (19)$$

$$\dagger E_{ADS} = \dagger E_{O_m/Pt_n} - E_{Pt_n} - \frac{m}{2}E_{O_2} \quad (20)$$

where $E_{O_m/Pt_n}$ is the energy obtained for the interacting system when the Pt nanoparticle is maintained rigid and $\dagger E_{O_m/Pt_n}$ is the energy obtained for the interacting system if the Pt nanoparticle is relaxed during the oxygen adsorption. $M$ and $N$ are the number of oxygen and Pt atoms. $E_{O_2}$ is the energy of an $O_2$ molecule in the triplet state, and $E_{Pt_n}$ is the energy for Pt nanoparticles relaxed without O atoms.

Table 1 shows the computed adsorption energies for the "Relaxing Pt" and "Freezing Pt" approaches, with differences of around 0.2 eV in the adsorption energies due to the effect of nanoparticle deformation after interaction with the adsorbates. The overall trends in the adsorption energies with increasing oxygen coverage are very similar with both approaches, with the main differences between both approaches happening for high O coverages.

To assess how the nanoparticle relaxation due to the interaction with the adsorbate changes the nanoparticle structure and the oxygen arrangement, we plot on Figure 5 spherical atomic distribution functions of Pt and O atoms using the atom in the centre of the nanoparticle as our reference. We present the atomic distribution function for the "Relaxing Pt" and "Freezing Pt" approaches using three different oxygen coverages.

**Table 1** The effect of Pt nanoparticle relaxation: Adsorption energies for Pt nanoparticles interacting with atomic O with and without geometry optimising Pt nanoparticles during the interaction with the adsorbate

| System | Relaxing Pt $\dagger E_{ADS}(eV)$ | Freezing Pt $E_{ADS}(eV)$ |
|---|---|---|
| $Pt_{55}$ O HCP (111) | -1.08 | -0.88 |
| $Pt_{55}$ Hemisphere 0.33ML | -1.07 | -0.84 |
| $Pt_{55}$ Hemisphere 0.66ML | -0.97 | -0.80 |
| $Pt_{55}$ Hemisphere 1.00ML | -0.89 | -0.74 |
| $Pt_{55}$ Nanoparticle 0.33ML | -1.06 | -0.85 |
| $Pt_{55}$ Nanoparticle 0.66ML | -0.94 | -0.74 |
| $Pt_{55}$ Nanoparticle 1.00ML | -0.82 | -0.50 |
| $Pt_{147}$ O HCP (111) | -1.11 | -0.85 |
| $Pt_{147}$ Hemisphere 0.15ML | -1.01 | -0.84 |
| $Pt_{147}$ Hemisphere 0.46ML | -1.03 | -0.86 |
| $Pt_{147}$ Hemisphere 0.91ML | -0.77 | -0.55 |

Figure 5 shows that the nanoparticle geometry due to the interaction with the adsorbates is highly dependent on the oxygen coverage. For the "Freezing Pt" approach with 0.33ML coverage, we see the presence of six distinct peaks, with four peaks representing Pt atoms and the other two oxygen atoms. The first peak at 2.74 Å shows the first Pt shell. For the second Pt shell, the peak at 4.00 Å represents Pt atoms in the centre of the (100) facet, while peaks at 4.78 Å and 5.39 Å represent atoms in the edges and vertices of the nanoparticle. The oxygen peaks for bridge (100) and HCP (111) adsorption sites are respectively represented at 5.57 Å and 6.10 Å far from the centre of the nanoparticle.

Still for the "Freezing Pt" approach, as we increase the oxygen coverage, the peak related to oxygen at the HCP (111) adsorption sites widens due to the O diffusion from HCP (111) to bridge sites in the edges and vertices of the nanoparticle. According to Han, Miranda and Ceder[37] and with our own calculations present in the supplementary information[†], the adsorption energies for these adsorption sites are relatively close, with bridge sites in edges of the nanoparticle being stronger than HCP(111) near the vertices. The similarity of the adsorption energies for the adsorption sites is responsible for an easy O diffusion[56]. The peak for the bridge (100) site remains almost constant. The diffusion of these O atoms is more difficult as bridge edge and top vertex sites are already occupied and the remaining adsorption sites, namely top sites in the nanoparticle edges and centre of (100) facets, adsorb oxygen much weaker than the initial position.

For the "Relaxing Pt" approach, we see that while the first peak remains in the same position for all O coverages, while the external Pt shell radially expands after the interaction with the adsorbates. For low coverages, such as 0.33ML, this expansion is the main modification and the characteristics cuboctahedral peaks described before are present. As the O coverage increases, the change in the nanoparticle geometry becomes more visible, and the oxygen radial distribution also changes. For the 1 ML coverage, we stop having distinct peaks for both, Pt and O atoms and a large overlapping region with Pt and O atoms appears, ranging from 5.25 Å to 6.25 Å, which indicates the formation of a Pt-O external shell instead of the regular O adsorbed on Pt nanoparticle behaviour. Figure 6 illustrates the final configuration for the 1

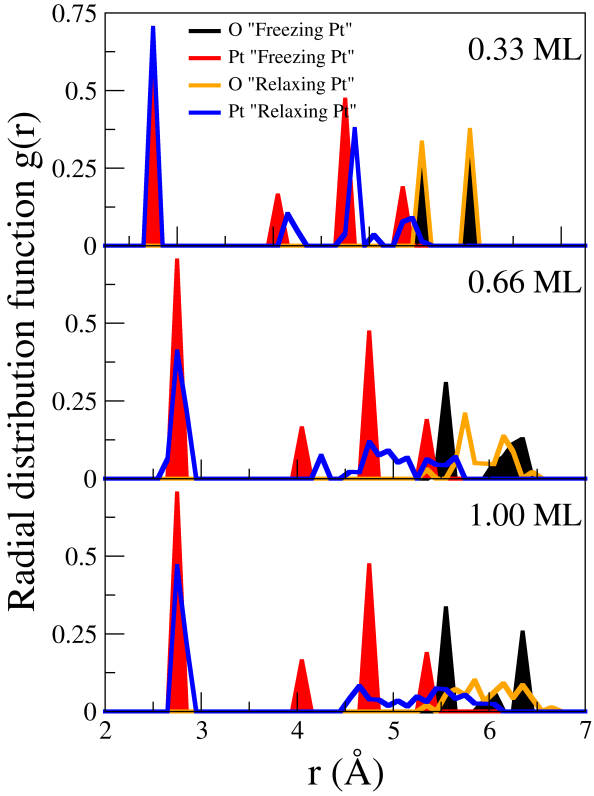


**Fig. 5** Radial distribution functions g(r) for "Relaxing Pt" and "Freezing Pt" approaches for 3 different oxygen coverages on $Pt_{55}$. Filled red (black) curves represent Pt (O) g(r) functions for the "Freezing Pt" calculations. Blue (orange) curves represent Pt (O) g(r) functions for "Relaxing Pt" calculations. The atom in the centre of the Pt nanoparticle is always used as the reference.

ML coverage with the "Relaxing Pt" and "Freezing Pt" approaches.

The results obtained with the "Relaxing Pt" approach show the sinking of the O atoms into the Pt nanoparticle structure as we increase the O coverage. This result agrees with observations of subsurface O atoms with increasing oxygen coverage, already observed experimentally[40,41] and in computational studies for nanoparticles[39,42] and slabs[43]. To accurately detect subsurface oxygen, our simulations would have to use a different approach and sample different initial configurations for the oxygen atoms. However, the sinking of oxygen atoms with increasing coverage can be an indication that at higher coverages the O adsorption starts to be unstable.

Our results indicate that if one is interested in assessing subsurface oxygen, the "Relaxing Pt" approach should be more suitable. Moreover, with increasing O coverage, there are some small variations in the effects of Pt relaxation due to the O adsorption. However, the main trends in adsorption energies per O atom with different coverages are very similar when calculated with both approaches. Thus, if one is mainly interested in the effect of the O coverage to the average bond strength between oxygen atoms and Pt nanoparticle, constrain Pt atoms movement during the adsorbate relaxation is a valid approach.

II) Hemispherical oxygen coverage.

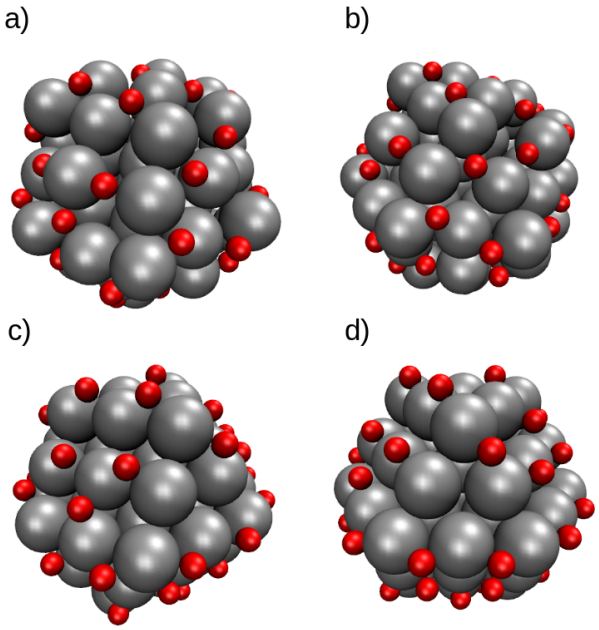


**Fig. 6** Final geometries for the 1 ML oxygen coverage with the a) and b) "Relaxing Pt" c) and d) and "Freezing Pt" approaches. Silver and red balls represent Pt and O atoms.

The cuboctahedral nanoparticle is symmetric, and the changes in the nanoparticle caused by the O adsorption are relatively local. Thus, as our second assumption, we consider that we do not need to cover the whole nanoparticle surface with O. We added oxygen only to one hemisphere of the nanoparticle, supposing that it would be enough to represent the problem we want to study.

**Table 2** Covering the whole nanoparticle vs hemispherical coverage: Adsorption energies for $Pt_{55}$ interacting with atomic O at different coverages with the whole $Pt_{55}$ surface and only one hemisphere covered with O

| System | Nanoparticle Coverage $E_{ADS}(eV)$ | Hemisphere Coverage $E_{ADS}(eV)$ |
|---|---|---|
| Relaxing Pt 0.33ML | -1.06 | -1.07 |
| Relaxing Pt 0.66ML | -0.94 | -0.97 |
| Relaxing Pt 1.00ML | -0.82 | -0.89 |
| Freezing Pt 0.33ML | -0.85 | -0.84 |
| Freezing Pt 0.66ML | -0.74 | -0.79 |
| Freezing Pt 1.00ML | -0.50 | -0.74 |

Table 2 shows the adsorption energies per O atom for the whole nanoparticle covered with O and for the hemispherical coverage. We computed these values using the "Relaxing Pt" and "Freezing Pt" approaches discussed before. In general, we see that this assumption does not change the behaviour of adsorption energies per O atom, being a valid approximation to reduce the computational cost.

The only significant change happens for our highest O coverage with the "Freezing Pt" approach, which should be treated carefully as previously demonstrated. For high O coverages, using a hemispherical coverage can induce an error in the final oxygen

distribution on the free/covered interface. For hemispherical coverages, the oxygens near the free/covered interface, which does not exist when the nanoparticle is fully covered, tend to move closer to facets free of oxygen to increase the distance between adsorbates.

III) Relaxing O atoms only for a specific facet.

Finally, we tested the effect of relaxing only a subset of O atoms. Here, we have tried to assess the O coverage effect for a single nanoparticle facet. We geometry optimised only the O atoms on a specific (111) facet and constrained the movement of all remaining O atoms, which were used to create an environment able to reproduce the O coverage effect.

We fixed the O surrounding atoms in the stable positions obtained for the single oxygen adsorption, constraining the movement of Pt and surrounding O atoms to drastically reduces the degrees of freedom in the geometry optimisation. We calculate the adsorption energies $\star E_{ADS}$, with a different methodology, demonstrated in equation 22, to obtain the results from a single facet.

$$\star E_{ADS} = E_{O_m/Pt_n} - E_{REF} - \frac{mm}{2} E_{O_2} \quad (21)$$

where, $E_{REF}$ is the energy for the reference system, illustrated on Figure7, $mm$ is the number of O atoms in the studied Pt facet, and $m$ is the total number of O atoms in the system. The energy $E_{O_m/Pt_n}$ can be calculated after the full geometry optimisation of all O atoms in the system or after the geometry optimisation of O atoms of one nanoparticle facet. In all the cases, we only covered one hemisphere of the nanoparticle.

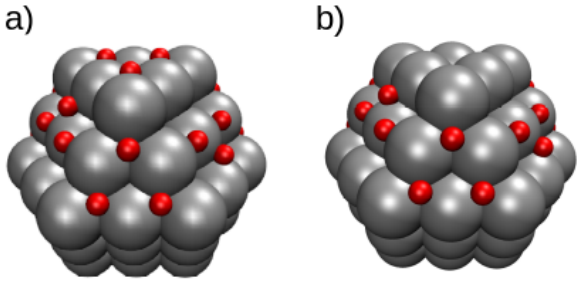


**Fig. 7** Illustration, on a $Pt_{55}$ nanoparticle, of the systems used to obtain a) $E_{O_m/Pt_n}$ b) $E_{REF}$, where the $E_{REF}$ structure is obtained by excluding the O atoms from the facet we are interested in studying

Table 3 shows the adsorption energies per O atom computed by geometry optimising all O atoms and just a nanoparticle facet. For the calculations that we geometry optimised all O atoms, we also show $E_{ADS}$ calculated with equation 19. The first two columns show that $E_{ADS}$ and $\star E_{ADS}$ are not comparable, as in one case we are assessing the adsorption energies for the whole nanoparticle including (111) and (100) facets, and for a single facet, and in the other case we assess a single (111) facet.

Comparing the final two columns, we see that relaxing only one nanoparticle facet is not enough to represent the oxygen coverage dependency in the adsorption energies. When we allow all O atoms to relax, the increase in the oxygen coverage induces a diffusion of O atoms from the initial hollow (111) sites to bridge and top sites in the edge and vertices of the nanoparticle. Thus, if we are not allowing all O atoms to relax, the atoms in the studied facet will find a different oxygen configuration near the nanoparticle edges and vertices.

**Table 3** Relaxing all O atoms vs Relaxing only the atoms on a specific facet: Adsorption energies per O atom for Pt nanoparticles interacting with atomic O at different coverages

| System | Relaxing all O $E_{ADS}(eV)$ | Relaxing all O $\star E_{ADS}(eV)$ | Relaxing O in the (111) facet $\star E_{ADS}(eV)$ |
|---|---|---|---|
| $Pt_{55}$ 0.33ML | -0.84 | -0.72 | -0.68 |
| $Pt_{55}$ 0.66ML | -0.80 | -1.24 | -0.72 |
| $Pt_{55}$ 1.00ML | -0.74 | -0.93 | -0.76 |
| $Pt_{147}$ 0.15ML | -0.84 | -0.89 | -0.91 |
| $Pt_{147}$ 0.46ML | -0.86 | -1.01 | -0.88 |
| $Pt_{147}$ 0.61ML | -0.87 | -0.91 | -0.76 |
| $Pt_{147}$ 0.91ML | -0.85 | -0.38 | -0.10 |

After our tests, we decided to study the interplay between the effect of oxygen coverage and Pt nanoparticle size using only the first two assumptions in our methodology. Thus, in the next section, we present the adsorption energies per O atom for different coverages in three nanoparticle sizes, by covering one hemisphere of the nanoparticle with oxygen and optimising all the oxygen positions, while keeping the Pt atoms frozen. Using this methodology, we are able to study the main trends in the adsorption energies per O atom for different oxygen coverages and nanoparticles sizes, separating the effects of oxygen cluster configuration and electronic changes in the nanoparticle surface due to increasing O coverage.

### 4.3 Interplay between nanoparticle size and O coverage

So far we have studied single atomic oxygen adsorption at different adsorption sites for Pt nanoparticles of increasing size and carefully assessed geometry optimisation methodologies to treat multiple oxygen adsorption with different coverages. Here, we employ the selected approach to study multiple oxygen adsorptions on the $Pt_{55}$, $Pt_{147}$, and $Pt_{309}$ nanoparticles with O coverages up to 1ML, where we define 1 ML coverage when we have the same number of O and surface Pt atoms.

Again, we started our simulations with O atoms placed at hollow HCP near the vertex of (111) facets and bridge sites near the edge of (100) facets. We increase the O coverage by adding one atom per facet up to the final coverage for each nanoparticle. For $Pt_{147}$ and $Pt_{309}$ nanoparticles, after filling with O the hollow HCP sites near the vertex, we start to use hollow HCP near the edges of the nanoparticle to build our initial guesses. The initial and final O configuration for each nanoparticle size and O coverage can be seen in the supplementary information.[†]

As oxygen adsorption energies are highly dependent on the adsorption site[21,22], we start our analysis showing on Table 4 the number of O atoms on each adsorption site for each nanoparticle size and oxygen coverage, where the numbers outside (inside) brackets represent the O configuration before (after) the geometry optimisations. We observe two distinct effects related to the interplay between Pt nanoparticle size effect and O coverage.

**Table 4** Number of O atoms present on each adsorption site for different nanoparticle sizes and oxygen coverages. Numbers outside (inside) brackets represent the O configuration before (after) the geometry optimisations.

| | HCP-V (111) | HCP-E (111) | Bridge-V (111) | Bridge-E (111) | Bridge-NE (100) | Bridge-V (100) | Top-E (100) |
|---|---|---|---|---|---|---|---|
| $Pt_{55}$ 0.33ML | 4 (4) | 0 (0) | 0 (0) | 0 (0) | 3 (3) | 0 (0) | 0 (0) |
| $Pt_{55}$ 0.66ML | 8 (1) | 0 (0) | 0 (7) | 0 (0) | 6 (6) | 0 (0) | 0 (0) |
| $Pt_{55}$ 1.00ML | 12 (2) | 0 (0) | 0 (10) | 0 (0) | 9 (6) | 0 (2) | 0 (1) |
| $Pt_{147}$ 0.15ML | 4 (4) | 0 (0) | 0 (0) | 0 (0) | 3 (3) | 0 (0) | 0 (0) |
| $Pt_{147}$ 0.30ML | 8 (8) | 0 (0) | 0 (0) | 0 (0) | 6 (6) | 0 (0) | 0 (0) |
| $Pt_{147}$ 0.45ML | 12 (12) | 0 (0) | 0 (0) | 0 (0) | 9 (9) | 0 (0) | 0 (0) |
| $Pt_{147}$ 0.61ML | 12 (3) | 4 (2) | 0 (9) | 0 (2) | 12 (12) | 0 (0) | 0 (0) |
| $Pt_{147}$ 0.76ML | 12 (3) | 8 (0) | 0 (9) | 0 (8) | 15 (15) | 0 (0) | 0 (0) |
| $Pt_{147}$ 0.91ML | 12 (0) | 12 (0) | 0 (12) | 0 (12) | 18 (16) | 0 (0) | 0 (2) |
| $Pt_{309}$ 0.09ML | 4 (4) | 0 (0) | 0 (0) | 0 (0) | 3 (3) | 0 (0) | 0 (0) |
| $Pt_{309}$ 0.17ML | 8 (8) | 0 (0) | 0 (0) | 0 (0) | 6 (6) | 0 (0) | 0 (0) |
| $Pt_{309}$ 0.26ML | 12 (12) | 0 (0) | 0 (0) | 0 (0) | 9 (9) | 0 (0) | 0 (0) |
| $Pt_{309}$ 0.35ML | 12 (12) | 4 (4) | 0 (0) | 0 (0) | 12 (12) | 0 (0) | 0 (0) |
| $Pt_{309}$ 0.43ML | 12 (12) | 8 (8) | 0 (0) | 0 (0) | 15 (15) | 0 (0) | 0 (0) |
| $Pt_{309}$ 0.60ML | 12 (11) | 16 (10) | 0 (1) | 0 (6) | 21 (21) | 0 (0) | 0 (0) |
| $Pt_{309}$ 0.78ML | 12 (3) | 24 (8) | 0 (9) | 0 (16) | 27 (27) | 0 (0) | 0 (0) |

The first effect is related to the difference in the percentage of a given adsorption site on different nanoparticles. As the nanoparticle size grows, adsorption sites near the vertices and edges represent a lower portion of the total number of sites. Thus, when comparing two nanoparticle sizes, the largest will have a higher number of weaker adsorption sites being used to obtain the same coverage. Consequently, when assessing the O coverage in terms of fraction of O monolayers, we will see a weakening in the adsorption energy per O atom due to the usage of weaker adsorption sites, which will be more pronounced as we increase the nanoparticle size.

The second effect is the oxygen diffusion during the geometry optimisations that happens for certain coverages. For all nanoparticle sizes, we see oxygen atoms moving from the initial adsorption sites if the coverages are higher than 0.6ML. For (111) facet, oxygen at the HCP (111) adsorption sites on the vertices and edges are destabilised with increasing coverages and diffuse to bridge sites in the vertices and edges of the nanoparticle. For (100) facet, oxygen remains stable for bridge sites near the edge for almost all coverages, with diffusions happening only for the highest O coverages in the covered/uncovered interface which is an artefact of adding O atoms to only one hemisphere. As explained in the previous section, the diffusion of oxygen atoms in the (100) facets is more difficult, as adsorption sites in the edges of the nanoparticle are occupied by O atoms from the (111) facets and the remaining sites bind oxygen much weaker than the initial position.

To assess how each effect contributes to the adsorption energy dependency on the oxygen coverage, we computed the single oxygen adsorption for each site and used these values to calculate the average O adsorption for the initial and final configurations, as follows:

$$\overline{E}_{ADS} = \frac{1}{m}\sum_{i}^{m} N_i E_{ADS(i)} \tag{22}$$

where $m$ is the total number of O atoms, $N_i$ is the number of atoms on adsorption sites similar to the adsorption site $i$, and $E_{ADS(i)}$ is the adsorption energy computed for a single oxygen adsorption at the site $i$. A list with the adsorption energies for each adsorption sites can be found in the supplementary information.†

Figure 8 shows the average adsorption energy $\overline{E}_{ADS}$ obtained for the initial and final O configuration presented on Table 4, and the adsorption energies per O atom $E_{ADS}$ for all the calculated O coverages and nanoparticle sizes.

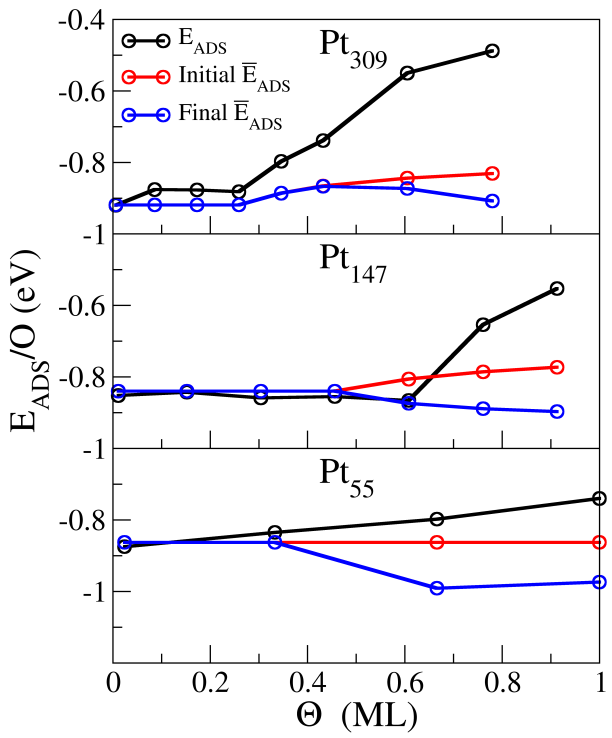


**Fig. 8** Adsorption energy averages $\overline{E}_{ADS}$ for initial (red segmented line) and final (blue segmented line) O configurations, and adsorption energies per O atom $E_{ADS}$ for several O coverages on $Pt_{55}$, $Pt_{147}$, and $Pt_{309}$ nanoparticles.

The *Initial* $\overline{E}_{ADS}$ represented by the red line on Figure 8 shows how the difference in the availability of adsorption sites for each nanoparticle size plays a role in the adsorption energy trend with increasing O coverage for each nanoparticle. For $Pt_{55}$, we achieve a 1ML O coverage using only HCP (111) sites at the vertex of the

nanoparticle and bridge sites for the (100) facet, which is responsible for the constant value of *Initial* $\overline{E}_{ADS}$. For $Pt_{147}$ and $Pt_{309}$, we obtain higher coverages by introducing weaker adsorption sites, which in turn reduce the average bond strength.

For all nanoparticle sizes, when the O coverage is higher than 0.6ML we see oxygen diffusions, which happen mainly from the HCP (111) adsorption sites to bridge sites in the vertices and edges of the nanoparticles. This effect increases the average bond strength, as the bridge sites in the edges between (111) and (100) facets have stronger binding energies than the initial HCP positions. The oxygen preference for adsorption sites in the edges and vertices of the nanoparticle with increasing O coverage was also previously observed with DFT[33,39] and MD[42] calculations, which similarly to our results, predicted a large concentration of oxygen in the edges of Pt nanoparticles and almost free terrace sites at (111) and (100) facets.

The assessment of these two effects and their evolution with the nanoparticle size, helps to understand the adsorption energy dependency on the O coverage and why each nanoparticle size seems to be affected differently by the O coverage increase. If we assess only the adsorption energies per O atom $E_{ADS}$ on Figure 8, we can assume that the O coverage increase has a larger effect as we grow the nanoparticle size. From Figure 8, we can see that the difference between $E_{ADS}$ for the highest and lowest oxygen coverage for a $Pt_{55}$ system is around 0.13 (eV/O), while for $Pt_{147}$ the difference is 0.30 (eV/O), and for $Pt_{309}$ it is 0.45 (eV/O).

Computing the difference between the average adsorption energy for single O adsorption *Final* $\overline{E}_{ADS}$ and the adsorption energy per O atom with the covered nanoparticles $E_{ADS}$, allows us to remove the contribution of the O cluster arrangement and observe to what extent increasing O coverage generates electronic interactions between adsorbates and modifications in the Pt surface which weaken the adsorption of extra O atoms. From Figure 8, we can see that the difference between *Final* $\overline{E}_{ADS}$ and $E_{ADS}$ for the highest oxygen coverage is 0.24 (eV/O) for $Pt_{55}$, 0.34 (eV/O) for $Pt_{147}$ and 0.44 (eV/O) for $Pt_{309}$. This shows that the observed weakening of the adsorption energies with increasing O coverage is controlled to a great extent by the electronic interactions between adsorbates and electronic changes in the Pt surface which weaken O adsorption.

To understand how the presence of O atoms changes the nanoparticle surface, we show on Figure 9 the d-band projected density of states for the surface Pt atoms on the covered hemisphere of $Pt_{55}$, $Pt_{147}$, and $Pt_{309}$ nanoparticles, for different O coverages. According to the d-band model, the adsorbate interaction with the metallic surface happens on a two stage process. The first stage is the renormalisation of the s and p orbitals of the adsorbate due to the interaction with the s and p orbitals of the metallic surface. As the s and p orbitals of metallic surfaces are delocalised, this part of the interaction should be relatively similar for all metallic surfaces. The second stage is the interaction of the renormalised s and p orbitals of the adsorbate with the d-band of the metallic surface, with the creation of bonding and antibonding orbitals. This part of the interaction is characteristic of each metallic surface, and the d-band centre acts as a good descriptor of the antibonding orbital and consequently the adsorption

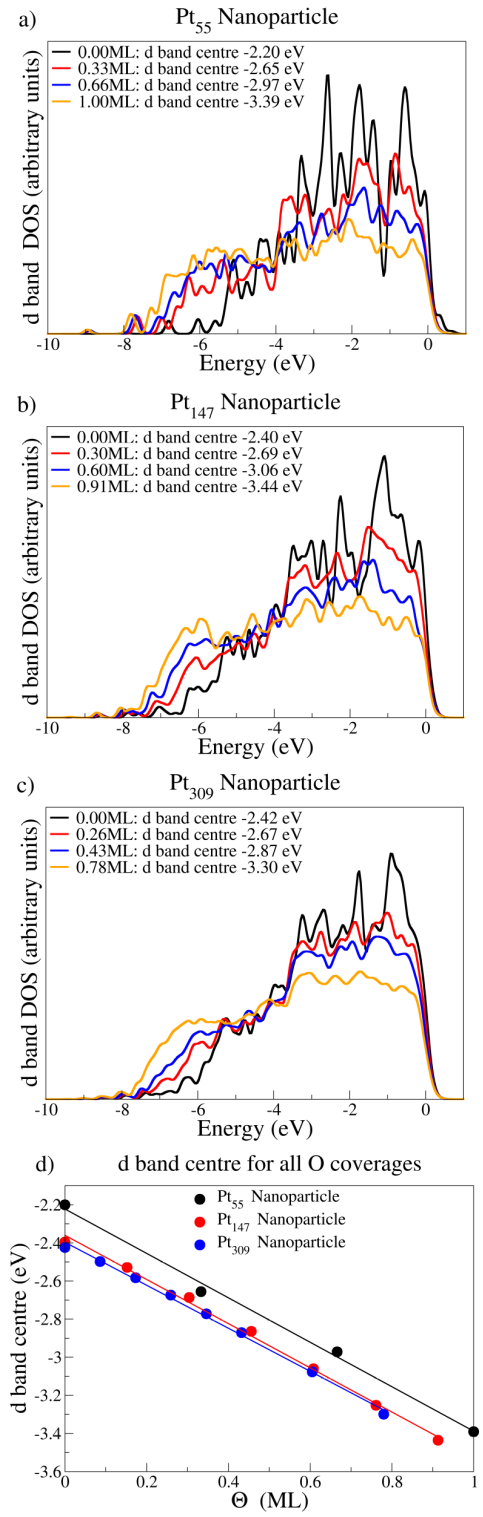


**Fig. 9** Density of states projected on the d-band of surface Pt atoms of cuboctahedral a) $Pt_{55}$, b) $Pt_{147}$, and c) $Pt_{309}$ nanoparticles with different O coverages. Figure d) shows the calculated d-band centre for each nanoparticle size as a function of the O coverage.

strength[5,12,13].

For all nanoparticle sizes, as we increase the O coverage, the d-band states near the Fermi level are reduced in intensity and the intensity of the states near the -6.0 eV region increases. The

peaks near -6.0 eV correspond to the overlapping orbitals between adsorbates and Pt surface. Additionally, to this effect we see a widening of the d-band states and consequently a downshift of the d-band centre. Figure 9 d) shows how the d-band centres change with increasing O coverage. For all nanoparticle sizes, we observed a linear correlation between the O coverage and the lowering of the d-band centre. Similar changes in the d-bands and d-band centre due to the adsorbate coverage were observed for Pt, Pd, Au (111) slabs interacting with O, CO, N, and used to explain the adsorption energy dependencies on the adsorbate coverage for all metallic surfaces and adsorbates[23–27].

For Pt nanoparticles, we observe that the downshifts in the d-band centres can be used to explain the weakening of the adsorption energies with increasing O coverage to some extent. When compared with the results obtained for metallic slabs[23–29], we obtained the same linear correlation between d-band centre and adsorbate coverage, while for the adsorption energies per O atom we see a non linear dependency on the O coverage. For Pt nanoparticles, we deal with a non-homogeneous O distribution through different adsorption sites and Pt facets, and we can use the d-band centre dependency on the O coverage only to qualitatively explain the physics about how the adsorbate coverage changes the electronic structure of the nanoparticle surface and consequently the bonding ability. However, we can not use the d-band centre of the Pt surface for different O coverages to linearly correlate the adsorption energies per O or to accurately predict the changes with increasing O coverage, showing that models for adsorbate-adsorbate interactions from calculations on metallic slabs should be used carefully when treating nanoparticles.

## 5 Conclusions

We carried out a study with large-scale DFT calculations on the interplay between the Pt nanoparticle size and O coverage effects. We described the implementation of angular momentum projected density of states (pDOS) within the ONETEP linear scaling DFT formalism and performed validation tests for simple systems such as an O atom and a CO molecule. We then computed single O adsorption energies for three adsorption sites on $Pt_n$ cuboctahedral nanoparticles with $n$ up 309 atoms. These calculations demonstrated the quick convergence of the adsorption energies for single O adsorption on Pt cuboctahedral nanoparticles, which are almost unchanged for nanoparticles larger than $Pt_{55}$. The size dependency on the adsorption energies correlates with the calculated d-band centre for (111) Pt facets on such nanoparticles, which were computed with the pDOS implementation previously described.

We performed a detailed analysis of different approaches of geometry optimisations used to study the oxygen coverage problem with DFT calculations, testing three approximations made to reduce the computational cost. We performed our tests with $Pt_{55}$ and $Pt_{147}$ nanoparticles and several O coverages. The first approximation is to maintain the Pt atoms in the nanoparticle in the optimised position found for an isolated nanoparticle. This approximation excludes the effects that the adsorbates create in the geometry of the nanoparticle, and greatly reduces the degrees of freedom in the geometry optimisation.

We showed that this approximation produces an almost constant shift in the adsorption energies of approximately 0.2 eV, maintaining the overall trends in adsorption energies per O atom with increasing O coverages and different nanoparticle sizes. The largest differences in adsorption energies happened for the higher computed O coverages. Additionally, the results observed when relaxing all Pt and O atoms, show a sinking of O atoms into the nanoparticle surface and considerable oxygen diffusion from their initial position as the O coverage increases. When the same systems are computed with a rigid Pt nanoparticle structure, only the O diffusion effect appears. These results show that the approximation is valid if one is mainly interested to study the dependency of adsorption energy per O atom with the O coverage and nanoparticle size, while for subsurface oxygen or higher O coverages studies the full relaxation should be more appropriate.

We also showed that it is possible to reproduce the results of covering a Pt nanoparticle with O by only covering one hemisphere of the cuboctahedral nanoparticle. This approach only produced significant changes for high O coverages, due to the migration of a few oxygen atoms near the free/covered interface, which does not exist when the nanoparticle is fully covered, towards the nanoparticle edges free of oxygen. As our third approximation, we tested the effect of relaxing only a subset of O atoms, optimising the O atoms for a single (111) facet while keeping all O the remaining O and Pt atoms in their initial positions. We saw that relaxing only a fraction of the O atoms was not enough to reproduce the final O positions for that facet and consequently the adsorption energies and O coverage dependency.

After these tests, the selected methodology was used to study the interplay between Pt nanoparticle size and O coverage, by computing a selection of coverages on $Pt_{55}$, $Pt_{147}$, and $Pt_{309}$ nanoparticles. We employed the first two assumptions, computing hemispherical O coverage and relaxing all O atoms with the Pt atoms frozen. We started our calculations placing O atoms at the hollow HCP near the vertices of (111) facets and bridge sites near the edges on (100) facets. As we increased the O coverage, we also used hollow HCP sites near the edges of (111) facets as initial positions for O atoms. In general, as we increase the O coverage the adsorption energy per O atom weakens and, when assessing the O concentration in terms of ML, this effect is more pronounced for larger nanoparticles.

We show that the differences observed in the adsorption energies per O atom due to the interplay between nanoparticle size and O coverage have three main causes. The first two are related with the adsorption sites where the O atoms are stable for each O coverage. For nanoparticles of different sizes, the proportion between the number of adsorption sites near the vertices, edges and centre is different. Thus, for each nanoparticle size, a same O coverage will be achieved with a different distribution of adsorption sites. For larger nanoparticles, higher coverages will consist of a higher proportion of weaker binding sites as compared with smaller nanoparticles, as the stronger adsorption sites are located on the edges and vertices of the nanoparticle. Secondly, for coverages higher than 0.6ML we see oxygen diffusions, mainly from the HCP (111) adsorption sites to bridge sites in the vertices and edges of the nanoparticles. The contribution of these two effects

into the O coverage dependency of the adsorption energies was computed by calculating the adsorption energy averages for initial and final O configurations with the results of single O adsorption for each adsorption site.

Finally, we calculate the difference between the average adsorption energy for the final O configuration calculated with single O adsorption data and the adsorption energy per O atom for O covered Pt nanoparticles, showing that the electronic interactions between adsorbates and the modifications that the O atoms create in the Pt nanoparticle surface electronic structure control to a great extent the weakening of the adsorption energies due to the O coverage increase. The results for the d-band projected density of states for the surface Pt atoms showed a linear correlation between increases in the O coverage and downshifts in the d-band centre, which illustrates how the presence of adsorbates modify the metallic surface and weaken the adsorption energies per O atom.

The trends we observe for d-band centre with increasing O coverage are similar to those obtained in the literature for slabs calculations[23–29], while the adsorption energy dependency on the O coverage differs from the trends for metallic slabs and are size dependent, showing the need of careful considerations to extend conclusions from metallic slabs to metallic nanoparticles. As the adsorption properties, which are key descriptors for catalytic systems, are dependent on the adsorbate coverage, we expect that the adsorbate coverage will play an important role under operating conditions. Thus, by bringing a detailed discussion about possible methodologies to tackle the problem with DFT calculations and by showing clear differences of the adsorbate coverage effect due to the nanoparticle size, we expect that our results will provide useful insights for understanding and developing better catalyst.

## 6 Conflicts of interest

There are no conflicts of interest to declare.

## 7 Acknowledgements

L.G.V acknowledges the support of Brazilian Government's Science Without Borders Programme (CNPQ: 206419/2014-7). J. A. acknowledges an EPSRC CASE PhD studentship supported by Johnson Matthey. We are grateful for access to the ARCHER national supercomputer via the UKCP consortium (EPSCRC grant number: EP/P022030/1). We are grateful to the UK Materials and Molecular Modelling Hub for computational resources, which is partially funded by EPSRC (EP/P020194/1). We are also grateful for access to the University of Southampton supercomputers Iridis3 and Irirdis4.

## References

1 M. Shao, Q. Chang, J.-P. Dodelet and R. Chenitz, *Chemical Reviews*, 2016, **116**, 3594–3657.

2 M. T. M. Koper, *Nanoscale*, 2011, **3**, 2054–2073.

3 A. J. Medford, A. Vojvodic, J. S. Hummelshøj, J. Voss, F. Abild-Pedersen, F. Studt, T. Bligaard, A. Nilsson and J. K. Nørskov, *Journal of Catalysis*, 2015, **328**, 36 – 42.

4 C. J. H. Jacobsen, S. Dahl, B. S. Clausen, S. Bahn, A. Logadottir and J. K. Nørskov, *Journal of the American Chemical Society*, 2001, **123**, 8404–8405.

5 J. K. Nørskov, J. Rossmeisl, A. Logadottir, L. Lindqvist, J. R. Kitchin, T. Bligaard and H. Jónsson, *The Journal of Physical Chemistry B*, 2004, **108**, 17886–17892.

6 A. U. Nilekar, Y. Xu, J. Zhang, M. B. Vukmirovic, K. Sasaki, R. R. Adzic and M. Mavrikakis, *Topics in Catalysis*, 2007, **46**, 276–284.

7 V. Stamenkovic, B. S. Mun, K. J. Mayrhofer, P. N. Ross, N. M. Markovic, J. Rossmeisl, J. Greeley and J. K. Nørskov, *Angewandte Chemie International Edition*, 2006, **45**, 2897–2901.

8 J. E. Sutton and D. G. Vlachos, *Industrial & Engineering Chemistry Research*, 2015, **54**, 4213–4225.

9 J. Cheng and P. Hu, *Journal of the American Chemical Society*, 2008, **130**, 10868–10869.

10 F. Abild-Pedersen, J. Greeley, F. Studt, J. Rossmeisl, T. R. Munter, P. G. Moses, E. Skúlason, T. Bligaard and J. K. Nørskov, *Phys. Rev. Lett.*, 2007, **99**, 016105.

11 B. Liu and J. Greeley, *The Journal of Physical Chemistry C*, 2011, **115**, 19702–19709.

12 B. Hammer and J. Nørskov, *Impact of Surface Science on Catalysis*, Academic Press, 2000, vol. 45, pp. 71 – 129.

13 J. K. Nørskov, F. Abild-Pedersen, F. Studt and T. Bligaard, *PNAS*, 2011, **108**, 937–943.

14 T. Bligaard and J. Nørskov, *Electrochimica Acta*, 2007, **52**, 5512 – 5516.

15 J. Greeley and M. Mavrikakis, *Nature Materials*, 2004, **3**, 810 – 815.

16 L. Ou, *Computational and Theoretical Chemistry*, 2014, **1048**, 69 – 76.

17 X. Xia, J. L. R. Yates, G. Jones, M. Sarwar, I. Harkness and D. Thompsett, *J. Mater. Chem. A*, 2016, **4**, 15181–15188.

18 I. Fampiou and A. Ramasubramaniam, *The Journal of Physical Chemistry C*, 2012, **116**, 6543–6555.

19 I. Fampiou and A. Ramasubramaniam, *The Journal of Physical Chemistry C*, 2013, **117**, 19927–19933.

20 L. G. Verga, J. Aarons, M. Sarwar, D. Thompsett, A. E. Russell and C.-K. Skylaris, *Phys. Chem. Chem. Phys.*, 2016, **18**, 32713–32722.

21 F. Calle-Vallejo, J. I. Martínez, J. M. García-Lastra, P. Sautet and D. Loffreda, *Angewandte Chemie International Edition*, 2014, **53**, 8316–8319.

22 J. Aarons, L. Jones, A. Varambhia, K. E. MacArthur, D. Ozkaya, M. Sarwar, C.-K. Skylaris and P. D. Nellist, *Nano Letters*, 2017, **17**, 4003–4012.

23 S. D. Miller and J. R. Kitchin, *Surface Science*, 2009, **603**, 794 – 801.

24 J. R. Kitchin, *Phys. Rev. B*, 2009, **79**, 205412.

25 Z. Xu and J. R. Kitchin, *The Journal of Physical Chemistry C*, 2014, **118**, 25597–25602.

26 N. İnoğlu and J. R. Kitchin, *Phys. Rev. B*, 2010, **82**, 045414.

27 M. J. Eslamibidgoli and M. H. Eikerling, *Electrocatalysis*, 2016, **7**, 345–354.

28 J. Bray, I. Skavdahl, J.-S. McEwen and W. Schneider, *Surface Science*, 2014, **622**, L1 – L6.

29 D. J. Schmidt, W. Chen, C. Wolverton and W. F. Schneider, *Journal of Chemical Theory and Computation*, 2012, **8**, 264–273.

30 R. B. Getman and W. F. Schneider, *ChemCatChem*, 2010, **2**, 1450–1460.

31 K. Frey, D. J. Schmidt, C. Wolverton and W. F. Schneider, *Catal. Sci. Technol.*, 2014, **4**, 4356–4365.

32 J. M. Bray, J. L. Smith and W. F. Schneider, *Topics in Catalysis*, 2014, **57**, 89–105.

33 G.-F. Wei and Z.-P. Liu, *Phys. Chem. Chem. Phys.*, 2013, **15**, 18555–18561.

34 V. Viswanathan and F. Y.-F. Wang, *Nanoscale*, 2012, **4**, 5110–5117.

35 V. Tripković, I. Cerri, T. Bligaard and J. Rossmeisl, *Catalysis Letters*, 2014, **144**, 380–388.

36 M. Shao, A. Peles and K. Shoemaker, *Nano Letters*, 2011, **11**, 3714–3719.

37 B. C. Han, C. R. Miranda and G. Ceder, *Phys. Rev. B*, 2008, **77**, 075410.

38 L. Li, A. H. Larsen, N. A. Romero, V. A. Morozov, C. Glinsvad, F. Abild-Pedersen, J. Greeley, K. W. Jacobsen and J. K. Nørskov, *The Journal of Physical Chemistry Letters*, 2013, **4**, 222–226.

39 R. Jinnouchi, K. K. T. Suzuki and Y. Morimoto, *Catalysis Today*, 2016, **262**, 100 – 109.

40 N. McMillan, T. Lele, C. Snively and J. Lauterbach, *Catalysis Today*, 2005, **105**, 244 – 253.

41 M. Teliska, W. E. O'Grady and D. E. Ramaker, *The Journal of Physical Chemistry B*, 2005, **109**, 8076–8084.

42 L. Gai, Y. K. Shin, M. Raju, A. C. T. van Duin and S. Raman, *The Journal of Physical Chemistry C*, 2016, **120**, 9780–9793.

43 Z. Gu and P. B. Balbuena, *The Journal of Physical Chemistry C*, 2007, **111**, 9877–9883.

44 A. A. Topalov, I. Katsounaros, M. Auinger, S. Cherevko, J. C. Meier, S. O. Klemm and K. J. J. Mayrhofer, *Angewandte Chemie International Edition*, 2012, **51**, 12613–12615.

45 C.-K. Skylaris, P. D. Haynes, A. A. Mostofi and M. C. Payne, *The Journal of Chemical Physics*, 2005, **122**, 084119.

46 A. Ruiz-Serrano and C.-K. Skylaris, *The Journal of Chemical Physics*, 2013, **139**, 054107.

47 C.-K. Skylaris, A. A. Mostofi, P. D. Haynes, O. Diéguez and M. C. Payne, *Phys. Rev. B*, 2002, **66**, 035119.

48 C.-K. Skylaris, A. A. Mostofi, P. D. Haynes, C. J. Pickard and M. C. Payne, *Computer Physics Communications*, 2001, **140**, 315 – 322.

49 B. Hammer, L. B. Hansen and J. K. Nørskov, *Phys. Rev. B*, 1999, **59**, 7413–7421.

50 K. Yang, J. Zheng, Y. Zhao and D. G. Truhlar, *The Journal of chemical physics*, 2010, **132**, 164117.

51 P. E. Blöchl, *Phys. Rev. B*, 1994, **50**, 17953–17979.

52 N. D. M. Hine, *Journal of Physics: Condensed Matter*, 2017, **29**, 024001.

53 A. A. Mostofi, P. D. Haynes, C.-K. Skylaris and M. C. Payne, *The Journal of Chemical Physics*, 2003, **119**, 8842.

54 N. D. Hine, J. Dziedzic, P. D. Haynes and C.-K. Skylaris, *The Journal of chemical physics*, 2011, **135**, 204103.

55 N. D. M. Hine, M. Robinson, P. D. Haynes, C.-K. Skylaris, M. C. Payne and A. A. Mostofi, *Phys. Rev. B*, 2011, **83**, 195102.

56 G. Peng and M. Mavrikakis, *Nano Letters*, 2015, **15**, 629–634.

57 L. Wang, A. Roudgar and M. Eikerling, *The Journal of Physical Chemistry C*, 2009, **113**, 17989–17996.

# Supporting Information

# DFT calculation of oxygen adsorption on platinum nanoparticles: Coverage and size effects

L.G. Verga,[a] J. Aarons,[a] M. Sarwar,[b] D. Thompsett,[b] A.E. Russell,[a] and C-K. Skylaris[a*]

[a] Department of Chemistry, University of Southampton, Highfield, Southampton SO17 1BJ, United Kingdom

[b] Johnson Matthey Technology Centre, Blounts Court, Reading, Berkshire, UK RG4 9NH

E-mail:* *c.skylaris@soton.ac.uk*

## 1 Coulomb-cutoff radius

We performed our calculations with the spherical Coulomb-cutoff to avoid any interaction between the system and the periodic images. We defined the minimum Coulomb-cutoff radius $r_{CC}$ after a convergence test with O adsorption at a hollow site in a (111) facet of a cuboctahedral $Pt_{55}$ nanoparticle with a diameter of approximately 11 Å. The following table shows how the adsorption energy changes with the Coulomb-cutoff radius.

**Table 1** Oxygen adsorption energies for different values of coulomb-cutoff radius.

| $r_{CC}$ (Å) | $E_{ADS}$ (eV) |
|---|---|
| 12 | -11.68 |
| 22 | -0.89 |
| 32 | -0.88 |
| 36 | -0.88 |
| 44 | -0.88 |

The first $r_{CC}$ value is larger than the maximum inter-atomic distance inside our system $rmax_{ij}$, while the second $r_{CC}$ value includes $rmax_{ij}$ and two times the NGWF radius $r_{NGWF}$. We only observed fluctuations in the adsorption energies happened for $r_{CC}$ between these limits. Thus, to ensure convergence within the Coulomb-cutoff radius, we used a minimum $r_{CC}$ which is calculated with the following equation:

$$r_{CC} = rmax_{ij} + 2r_{NGWF} + a \tag{1}$$

where we add the maximum inter-atomic separation, two times the NGWF radius, and a constant value $a$ of at least 5 Å to account for Gibbs oscillations, as the Cutoff Coulomb operator is computed in reciprocal space.

## 2 Initial and Final O distribution

As discussed in the main article, the initial O distribution with a given O coverage is different for each nanoparticle size, as the ratio between adsorption sites in the edges and vertices of the nanoparticle and terrace sites is size dependent. Figure 1 shows the initial and final O configuration for $Pt_{55}$ with three different values of O coverage. At this nanoparticle size, we reach a 1.00ML coverage using only HCP vertex sites for (111) facets and Bridge sites near the edges for (100) facets. For 0.66ML and 1.00ML coverages, we clearly see O atoms moving from the initial HCP (111) adsorption sites to bridge sites in the vertices of the nanoparticle after the geometry optimisation.

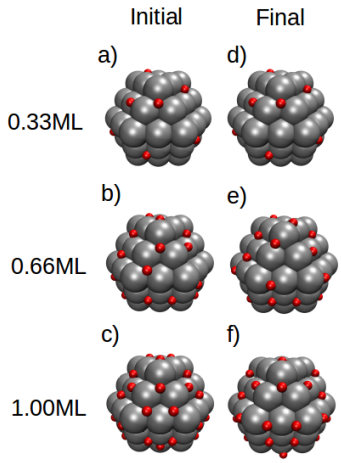


**Figure 1** $Pt_{55}$ nanoparticle covered with atomic oxygen on different coverages, where a), b), c) show initial O configuration and d), e), f) show the O configuration after geometry optimisation. Silver (red) balls represent Pt (O) atoms.

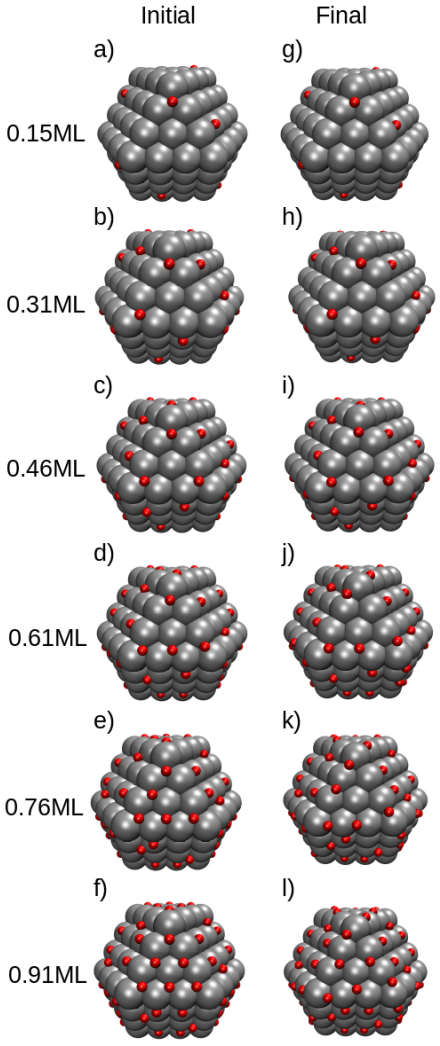


**Figure 2** $Pt_{147}$ nanoparticle covered with atomic oxygen on different coverages, where a), b), c), d) show initial O configuration and e), f), g), h) show the O configuration after geometry optimisation. Silver (red) balls represent Pt (O) atoms.

Figure 2 shows the initial and final O configuration for $Pt_{147}$ nanoparticles with different O coverages. The O coverage up to 0.46ML is obtained by adding one O atom to a HCP vertex (111) site and one O atom to a Bridge site near the edge of (100) facet. For higher O coverages, we also use HCP edges (111) adsorption sites. Similarly to the results obtained for $Pt_{55}$, we only see oxygen movement between adsorption sites for systems with O coverages equal or higher than 0.60ML.

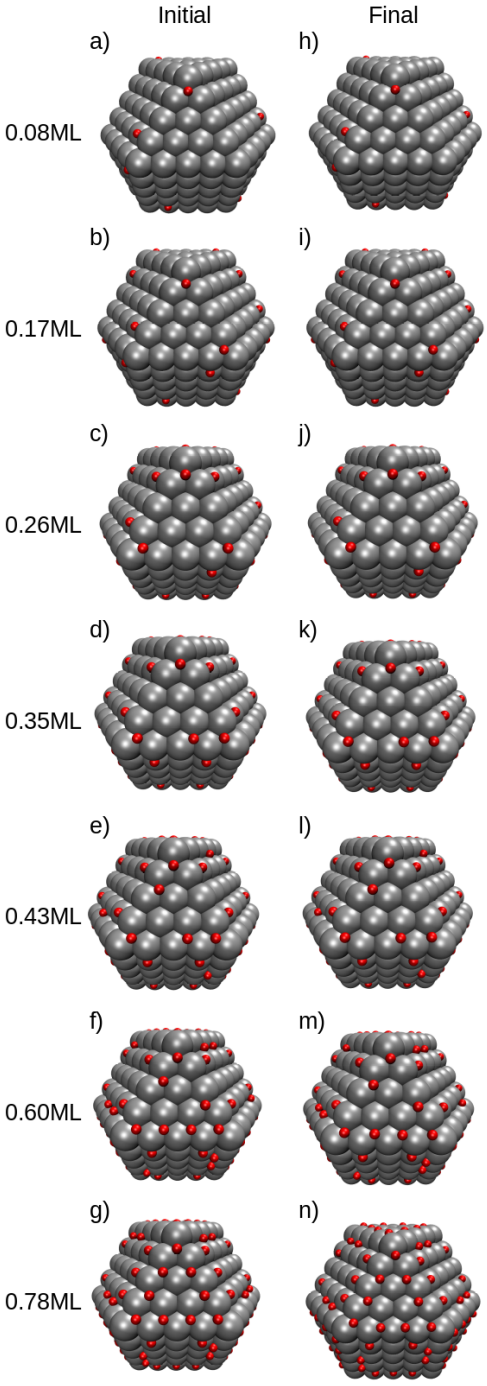


**Figure 3** $Pt_{309}$ nanoparticle covered with atomic oxygen on different coverages, where a), b), c), d), e) show initial O configuration and f), g), h), i), j) show the O configuration after geometry optimisation. Silver (red) balls represent Pt (O) atoms.

For $Pt_{309}$ nanoparticles, as illustrated on Figure 3, we see significant changes between initial and final O config-

uration only for the systems with 0.78ML O coverage. For 0.6ML O coverage, we see small changes between initial and final O configurations, while for systems with lower coverage the initial and final O configuration are identical.

We calculate single O adsorption for each adsorption site present on initial or final O configurations for all nanoparticle sizes and O coverages. These values are used in the main article to calculate the average adsorption energy for the initial and final O configuration. Table 2 shows the adsorption energy for different nanoparticle sizes and adsorption sites.

**Table 2** Adsorption energies for single O adsorption on different adsorption sites and nanoparticle sizes, where NE and NC are non-existent and non-computed adsorption sites.

| | $Pt_{55}$ | $Pt_{147}$ | $Pt_{309}$ |
|---|---|---|---|
| | $E_{ADS}$ (eV) | $E_{ADS}$ (eV) | $E_{ADS}$ (eV) |
| HCP-V (111) | -0.87 | -0.85 | -0.92 |
| HCP-E (111) | NE | -0.61 | -0.69 |
| Bridge-V (111) | -1.13 | -1.00 | -1.08 |
| Bridge-E (111) | NC | -0.90 | -0.90 |
| Bridge-NE (100) | -0.85 | -0.83 | -0.91 |
| Bridge-V (100) | -0.98 | NC | NC |
| Top-E (100) | -0.36 | -0.28 | NC |

For all the nanoparticles we examined, we see that adsorption energies for Bridge sites in the vertices and edges of the nanoparticle are comparable or stronger than those obtained for HCP sites, making easier the O movement between these two adsorption sites. For the (100) facet, the only adsorption site as strong as the initial Bridge sites located near the edge of the nanoparticle is the adsorption site in the vertex between the (100) and (111) facets. However, after geometry optimisation, the sites in the edges and vertices of the nanoparticle are occupied by O atoms moving from the HCP (111) sites. Thus, as these sites are occupied, and top sites in the edge of (100) facets are much weaker than the initial bridge sites near edge, almost no O diffusion happens for (100) facets.

## Table of contents entry

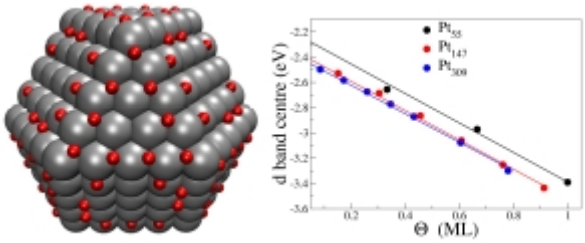


DFT calculations are used to simultaneously explore the effects of nanoparticle size and coverage for O adsorption on Pt nanoparticles.